Effects of Spectral Density on the Azide Vibrational Transition in Water versus D_2O

Majid Hassani,[a] Derek C. Moore,[a] Matthew G. Roberson,[a] Somnath Kashid,[a] and Matthew J Tucker[a,*]

[*]Corresponding Author, Matthew J Tucker. Email: mtucker@unr.edu. Tel: 7757844376

[a]*Department of Chemistry, University of Nevada, Reno, Nevada, 89557, United States*

Abstract

Water and D_2O have distinct spectral densities resulting from isotopic shifts associated with their vibrational manifold. Two-dimensional infrared, pump-probe, and transient grating spectroscopies were employed to directly measure the vibrational dynamics for the azide transition of NaN_3 within solutions of water and D_2O. Although the frequency correlation time revealed minimal variation, a linear correlation between lifetime and the optical density of the solvent background was uncovered. Thus, a predictive model of the lifetime was proposed. These findings highlight the importance of spectral density of the solvent and its role in the pathways of energy dissipation for vibrational probes.

Keywords: (azide probe, vibrational reporter, vibrational lifetimes, spectral density)

1. Introduction

Infrared reporters like nitriles and azides have become popular probes for studying biomolecules because of their sensitivity to local environments, chemical stability, small size, and relatively localized transitions[1-7]. In particular, ultrafast measurements of the stretching mode of the nitrile group in a variety of biological systems have provided insight into site-specific structural dynamics[4,8-10]. Since both the azide and nitrile transitions are found in a spectrally transparent region of most biological molecules, several studies have benefited from the isolated and relatively sharp spectral feature to investigate β-amyloid aggregation[11], drug–enzyme interactions[8,12], peptide folding[1,13], and other biological processes[14,15]. Despite having a wide variety of applications, the relatively small absorption cross section (~200 M^{-1} cm^{-1}) of the nitrile vibrational transition makes this probe challenging to utilize in nonlinear IR spectroscopy due to the balance between the higher concentrations needed to obtain sufficient signal strength and the lower concentrations that are acceptable for biological systems. However, several alternatives have been developed recently[16-18] so that the most suitable vibrational reporter can be selected for the desired application within a biological system.

One such alternative, the azido- group, has shown significant promise in capturing small changes in the vibrational dynamics for the nucleoside 2′-azido-2′-deoxyuridine[19], peptides and proteins[20], as well as enzyme dynamics[21]. The absorption cross section of the azide transition

is much larger (~10-15x) than that of nitrile group[20], enabling the use of lower concentrations for biological systems. Specifically, the aliphatic azido- substitutions are stable under most conditions and often avoid accidental Fermi resonances[22], allowing the azido- reporter to respond to the local environment more effectively in peptides, proteins, and nucleosides[19,23,24]. Both the azide transition and the nitrile transition have many similar spectral properties and a direct comparison of these probes has been documented[5]. Moreover, when combined as a "probe pair", distances between specific sites in biomolecules can be determined[4]. The sensitivity of the vibrational frequency to hydrogen bonding and the local electric field offers another way to probe structural dynamics in biosystems. The frequency dependence on its surroundings translates to capturing structural motions of enzymes[25] and ligand binding[13] by utilizing the frequency-frequency correlation function. Overall, the sensitivity of these reporters to the local environment and hydrogen bonding provides an avenue to track these structural dynamics by two-dimensional infrared methods via chemical exchange and spectral diffusion[26].

Two-dimensional infrared (2D IR) photon echo spectroscopy is an effective method for observing vibrational dynamics, including spectral diffusion[27-29], inter-mode coupling[30], conformational analysis[31], and energy transfer[30,32,33]. Although thermal energy flow to the solvent environment is often considered to appear in contributions to the inhomogeneous frequency-frequency correlation decay, it has been documented that the solvent environment can affect the vibrational lifetimes[34]. Specifically, the coupling to the bath depends on the "spectral density" of the modes.[35] The spectral density is dependent on the number of vibrational modes of the solvent overlapping the spectral region of interest and/or the concentration of oscillators within that specific region. Both contribute to direct interactions such as coupling and energy transfer or dissipation. For example, the density of states of D_2O is two times larger than water near 2000 cm^{-1} but the specific mode coupling plays a role resulting in a much longer lifetime than water.[35] In particular, the coupling of the water combination band around 2115 and the azide transition provide a direct relaxation pathway but the closest band to D_2O is the edge of bending mode at 2360 cm^{-1}. Pump-probe and transient grating techniques can provide additional information on the structure and dynamics of solvated molecules and on how the characteristics of the solvent affect vibrational energy loss[35].

In this manuscript, we present a systematic study of sodium azide (NaN_3) in various D_2O/H_2O solutions. We used 2D IR, pump-probe, and transient grating measurements to examine the vibrational lifetimes and frequency-frequency correlation decays of the azido- transition upon variation of the solvent spectral density. Furthermore, we developed a predictive model for the vibrational lifetimes based on the spectral density of the water/D_2O solution. While this study focuses on a small-molecule system, the observed bath coupling model can be served as a guide for tuning the vibrational lifetime in larger biomolecular systems.

2. Experimental methods

Solutions of approximately 20-30 mM NaN_3 in water and deuterated water were prepared for both linear FTIR and 2D IR experiments. The solvent was varied via serial dilutions to measure a range of conditions between 100% water and 100% D_2O. Linear infrared spectra were collected using a ThermoNicolet 6700 FTIR spectrometer equipped with a liquid nitrogen-cooled mercury cadmium telluride detector. To collect higher sensitivity spectra and correct the baselines more accurately, the IR beam was routed into a home-built setup[36]. For the enhancement of baseline

correction, the two-compartment CaF_2 sample cell with a 56 μm Teflon spacer was utilized, ensuring that measurements of the reference and the sample were performed under the same conditions. A single beam spectrum is collected by an automated translation stage that moves the sample cell between the reference and the sample side to account for drift and stability[37]. All measurements were conducted in a nitrogen-purged chamber at room temperature (~20°C). All FTIR spectra were averaged for 128 scans. To determine the full width at half maximum (FWHM), each transition was fitted to a Gaussian profile,

$$OD(\omega) = A * e^{-4*ln(2)*\frac{(\omega-\omega_C)^2}{(FWHM)^2}}. \quad (1)$$

The 2D IR spectra presented in this work were obtained using a combination of both pulse shaper based 2D IR setup and a box-car photon echo 2D IR spectrometer setup. For the 2D IR pulse shaping, mid-IR pulses with an 80 fs Gaussian pulse width and centered at 4902 nm were split into pump and probe beams with a CaF_2 wedged window. The pump pulse, ~15 μJ, was directed through a germanium acousto-optic modulator (AOM) based pulse shaper. The pulse shaper produced a collinear pair of compressed pump pulses with variable delays (τ), which were scanned to generate the pump axis of the 2D IR spectra. The pump and probe pulses were then spatially overlapped and focused at the sample. An automated translation stage was used to set a fixed temporal delay or waiting time T_w to adjust the timing between the pump and probe pulses. The box-car 2D IR photon echo setup has been described elsewhere[38]. To acquire absorptive spectra, the rephasing and nonrephasing 2D frequency spectra were properly phased and combined. The waiting time, T, varies by using different delays between the second and third pulse. The vibrational relaxation times (τ) were measured from the decay of the on-diagonal signal strengths of the $0 \rightarrow 1$ transition in the 2D IR spectrum at different waiting times and fitted to an exponential decay,

$$I_{2D}(T) = A_0 e^{-T/\tau}. \quad (2)$$

Transient grating experiments were performed similarly to the 2D IR experiments, but with k_1 and k_2 fixed while k_3 and the local oscillator were moved synchronously in 10 fs steps to vary the delay time. Solvent transient grating spectra were subtracted from the azide spectra. Similarly to the 2D IR experiments, relaxation times were obtained from the decay of the $0 \rightarrow 1$ transition. Additionally, the decay of the azide vibrational transition in water observed in the transient grating experiment was fit to a function containing both population and reorientation relaxation [39], given by

$$f(T) = ae^{-T/T_1}\left((4/9)e^{-T/T_R} + (5/9)\right). \quad (3)$$

Pump-probe data were collected by blocking k_1 and k_3, then directing the local oscillator through the sample to serve as the probe while k_2 acted as the pump. Data points were collected in 10 fs steps and then binned with five points per bin. The decay of the $0 \rightarrow 1$ transition was again used to determine vibrational relaxation times. Kinetic traces and fits were generated by averaging the traces of the three wavenumbers nearest to the transition peak. Using a combination of a half-wave plate and polarizer on each beam, the angle between the pump and the probe was set at the magic angle (54.7°) to eliminate any rotational contributions to the lifetime.

Table 1. FWHM of the NaN_3 vibrational transition in D_2O/H_2O solution.

D_2O %	100 %	90 %	80 %	70 %	60 %	50 %	40 %	30 %	20 %	10 %	0 %
FWHM (cm^{-1})	18.8 ± 0.1	19.3 ± 0.1	19.8 ± 0.1	20.3 ± 0.1	21.0 ±0.1	21.5 ± 0.1	22.2 ± 0.1	22.9 ± 0.1	24.1 ± 0.1	25.5 ± 0.1	27.1 ± 0.2

3. Results and Discussion

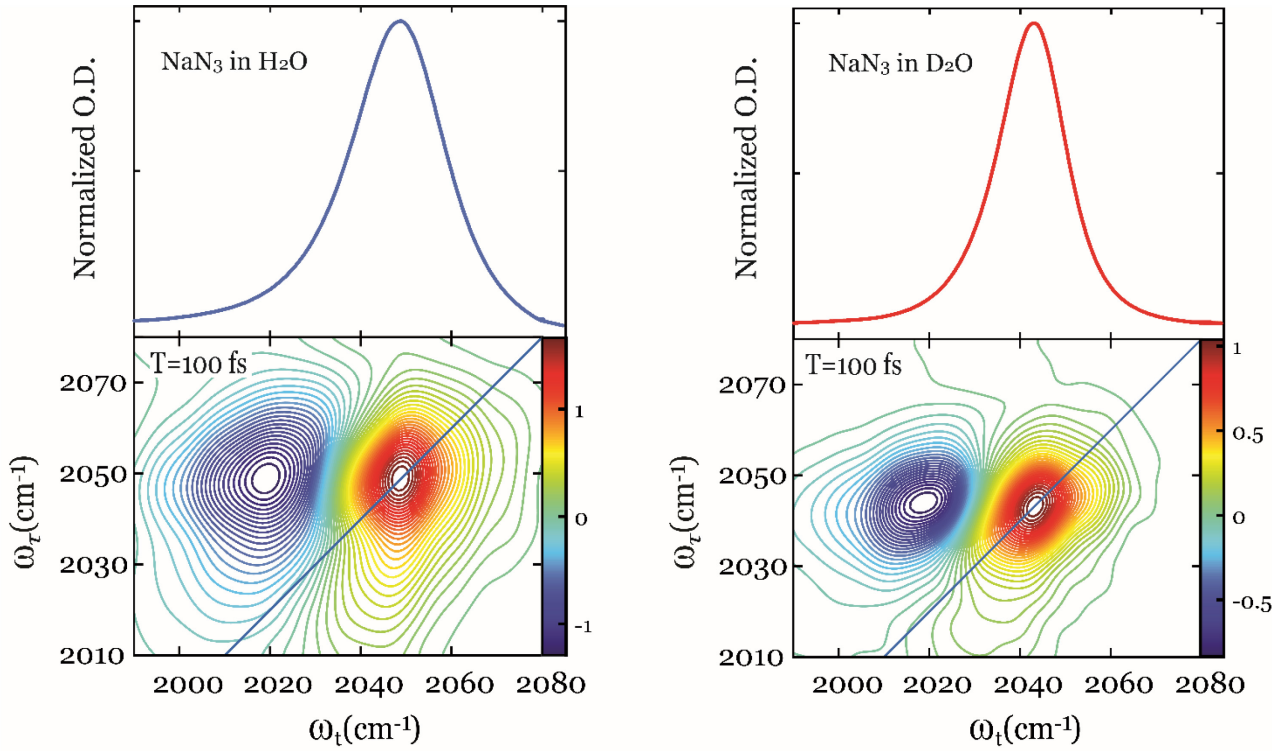

Figure 1. Normalized FTIR spectrum of NaN_3 (top panel) in (left) H_2O and (right) D_2O along with the corresponding absorptive 2D IR spectra (bottom panel) at 100 fs.

Linear FTIR and 2D IR experiments were performed on NaN_3 in different D_2O/H_2O solutions with systematic changes in solvent ratio to understand the solvent influence, i.e. the 'spectral density', in the azido- transition region of the spectrum. A single transition associated with the azide antisymmetric stretch is observed in the linear FTIR spectra of NaN_3 in pure H_2O and deuterated water (D_2O) (top panel, Figure 1). These transitions are observed at 2049 cm^{-1} and 2043 cm^{-1} in water and D_2O, respectively, indicating a 5 cm^{-1} redshift due to the secondary isotopic effect and/or a resonance interaction with the bending mode of water. The calculated full width at half maximum (FWHM), obtained from fitting to Gaussian line shapes, is 27.1 ± 0.2 cm^{-1} in water. The linewidth is approximately 1.45-fold narrower in D_2O than H_2O as a result of stronger hydrogen bonding, decreasing the frequency distribution and illustrating the importance of hydrogen bonding to the relaxation pathway[40,41]. Table 1 shows the variations in the FWHM of the azido-transition in different ratio D_2O/H_2O solutions. As the percentage of deuterated water decreases, the linewidth increases as the average rate of hydrogen bonding increases over time[42-

44]. This increase in hydrogen bonding rate causes the structural distribution to become larger, i.e. it generates a larger inhomogeneous distribution of states.

The 2D IR spectra of NaN_3 in water and D_2O at 200 fs waiting times are also shown in the bottom panels of Figure 1. Akin to the linear IR spectrum, the azide $\nu = 0 \rightarrow \nu = 1$ transitions appear along the diagonal at $\omega_t = \omega_\tau = 2049$ cm^{-1}, and $\omega_t = \omega_\tau = 2043$ cm^{-1} in H_2O and D_2O, respectively. The negative contours red-shifted along the ω_t axis represent $\nu = 1 \rightarrow \nu = 2$ transitions and represent the anharmonic nature of the oscillations. The diagonal anharmonicities of the azide transitions in water and deuterated water are approximately 22 ± 2 cm^{-1} and 25.2 ± 0.4 cm^{-1}, suggesting that anharmonicity is only slightly affected by the solvent molecules, which has been observed for carbonyl oscillators[45].

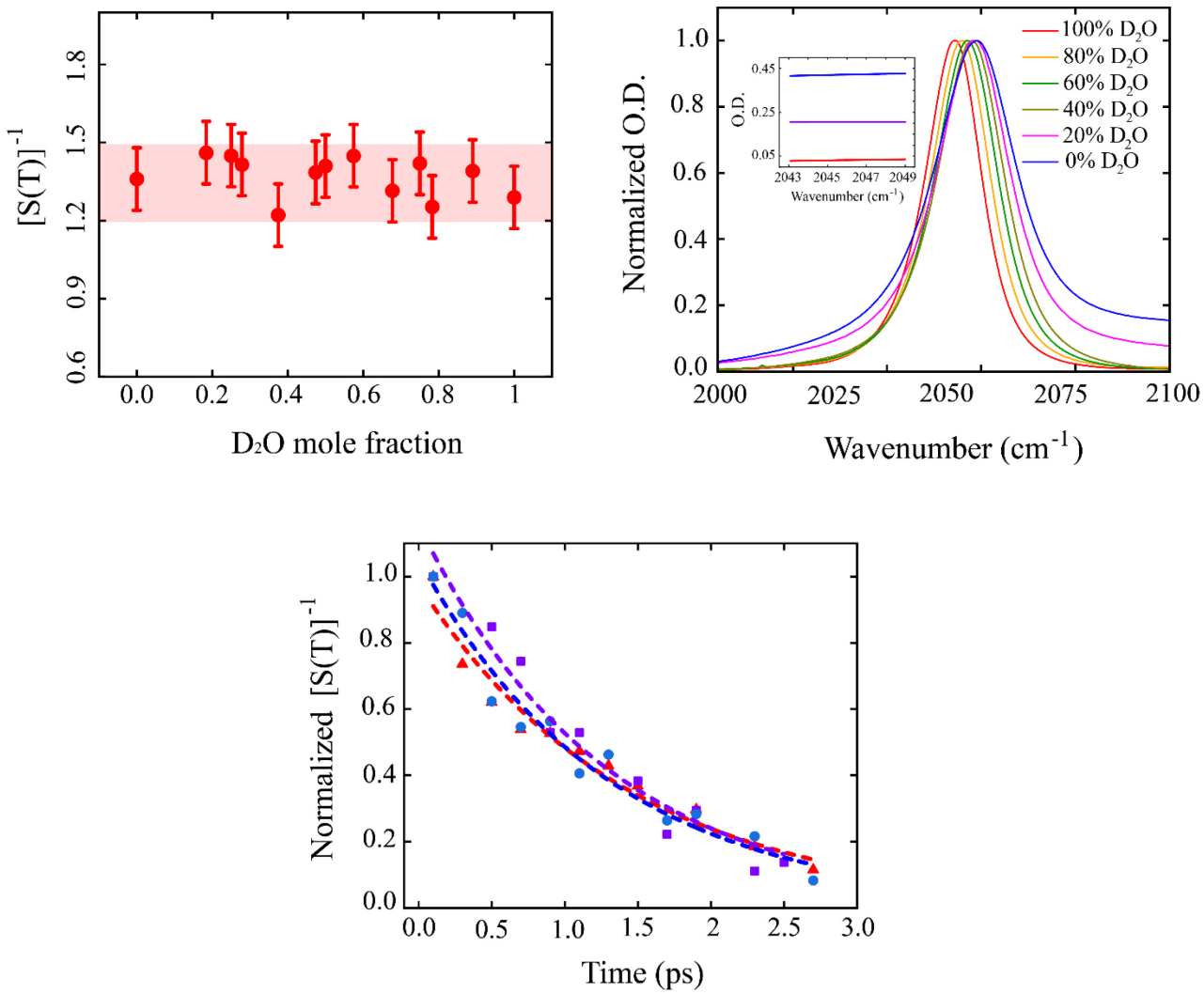

Figure 2. (Top Left) Inverse slope [S(T)$^{-1}$] vs D_2O mole fraction. (Top Right) Infrared spectra for NaN_3 in D_2O/H_2O solution with varying D_2O percentage. The inset shows the FTIR optical density of (red) pure D_2O, (blue) H_2O and (purple) 50:50 (volume:volume) solutions zoomed into the region of interest. (Bottom Center) Representative CLS correlation decays for D_2O (red triangles), H_2O (blue circles), and 50:50 D_2O:H_2O (purple squares).

Information about the relaxation dynamics of vibrational reporter can be obtained by measuring the spectral diffusion as a function of waiting time[46-49]. As waiting time increases the peaks become more circular, indicating a loss of frequency correlation caused by structural

dynamics. The center line slope (CLS) method is a useful technique for quantifying the loss of frequency correlation and provides direct access to the frequency-frequency correlation decay [49]. Using the CLS method, the loss of frequency correlation of the vibrational transition can be measured as a function of waiting time, T. The correlation decay is plotted as the inverse slope of the CLS, $[S(T)]^{-1}$, and fitted to a single exponential decay function,

$$[S(T)]^{-1} = A_0 e^{-T/\tau}, \quad (4)$$

where τ represents the correlation decay constant. This function has no fixed offset, as opposed to the complete frequency-frequency correlation function which may contain a static component. For this work, the CLS correlation decay lifetime for the azide probe in different D_2O/H_2O ratio solutions were determined. The top left panel of Figure 2 shows the CLS decay constant as a function of D_2O mole fraction and reveals very small changes in frequency-frequency correlation function dynamics and/or inhomogeneity with varying D_2O/H_2O content. CLS decay constants are calculated from the slopes of positive- and negative-going peaks, as well as for the slope of the zeroth contour between the peaks. The standard deviation of all the values is used to generate the error bars. The average value of the CLS correlation decay is approximately 1.4 ± 0.1 ps, and all CLS decay values for different solutions are within the experimental error. Representative CLS correlation decays for D_2O, H_2O, and 50:50 D_2O:H_2O are shown in the bottom panel of Figure 2. The faint red shadow region indicates the area associated with the range of values observed. This result suggests that the inhomogeneous contribution to the FWHM in the FTIR spectral line shape does not vary for these different solutions. Thus, the fast relaxation pathways, associated with the population relaxation and the reorientation dynamics, must significantly impact the observed differences in the FWHM (Figure 2 – top right). These dynamics will be detected from the different pump-probe spectroscopies and compared to the intensity decay of the 2D IR spectra. A systematic red shift is also observed in the azide peak with increasing D_2O mole fraction. This shift in the vibrational frequency is a result of less hydrogen bonding species within the ensemble average, shifting toward the direction with no hydrogen bonding as previously reported for azido-probes in tetrahydrofuran[19].

The decrease in $\nu = 0 \rightarrow \nu = 1$ diagonal peak intensity with increasing waiting time in 2D IR spectroscopy is directly related to the vibrational relaxation, i.e. population relaxation and reorientation time, of the probe[39,50]. The reorientation component can sometimes be neglected if it is long compared to the population relaxation. To assess one of these relaxation pathways, the population relaxations were obtained free of reorientation components. Pump-probe spectroscopic measurements were performed with the relative orientation between the pump and probe beam set to the magic angle (54.7°). The decay curve is fitted with a single exponential function,

$$I_{PP}(T) = A_0 e^{-T/\tau}. \quad (5)$$

The left panel of Figure 3 shows the pump-probe decay of the $\nu = 0 \rightarrow \nu = 1$ azide transition in pure D_2O and H_2O. The fits of the decays yielded time constants of 2.2 ± 0.1 ps in D_2O and 0.52 ± 0.02 ps in H_2O. These results indicate the vibrational lifetime of the azide probe is 4.2 times shorter in water. The reason for this vast difference in vibrational lifetime between water and D_2O is due to the spectral density of the solvents. Spectral density refers to the distribution of vibrational frequencies resonant with the vibrational transition and their corresponding coupling into the molecular system. The collision-induced mixing of internal modes of the system dramatically affects the dissipation pathway. In the context of vibrational lifetimes, the spectral density describes the number of vibrational modes accessible, i.e. in resonance, to the vibrational

transition to quickly divert energy and damp the oscillation. In the case of water and D_2O, the difference in vibrational lifetimes arises from the disparity in their respective spectral densities shown by the optical densities of the solvents in the region of the interest (Figure 2 – inset). D_2O exhibits a lower spectral density compared to water in the azide region due to the shift of the combination band, 2075 cm^{-1}, of water out of the spectral region. Thus, azide in D_2O maintains its vibrational energy for a longer time compared to azide in water. This is because the energy has less propensity to spread out to other modes or transfer to the surrounding environment or bath.

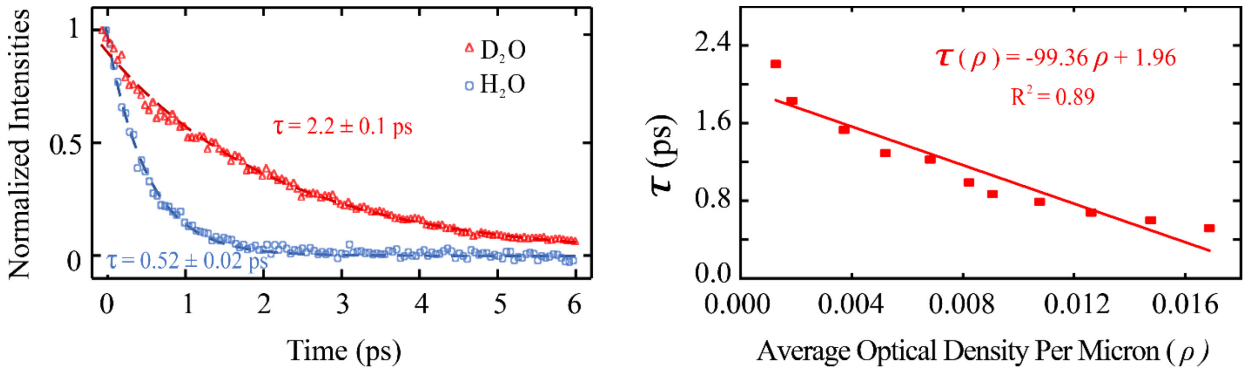

Figure 3. (Left) Kinetic traces and fits of the pump probe magic angle spectra for NaN_3 in pure (red triangles) D_2O and (blue circles) H_2O. (Right) Azide vibrational population lifetime determined from magic angle pump probe as a function of average optical density per micron (100% D_2O to 100 % H_2O from left to right).

To systematically assess the effects of spectral density, the vibrational lifetime for the azide transition was determined from the magic-angle pump-probe intensity decay for different D_2O/H_2O ratios. Interestingly, the vibrational lifetime of the azide probe shows a linear correlation as a function of the average optical density of D_2O/H_2O solution within the spectral region of interest (right panel of Figure 3). The average optical density was determined by calculating the mean of the optical densities measured between 2043 cm^{-1} and 2049 cm^{-1} of the bath alone, where NaN_3 transition is typically observed. Additionally, a linear trend follows with the mole fraction of H_2O, which is important to understand the HOD contribution in the solvent system. With the help of this semi-empirical equation,

$$\tau(\rho) = -99.36\rho + 1.96, \quad (6)$$

the population relaxation lifetime ($\tau(\rho)$) can be predicted depending on the average optical density per micron (ρ) of the solvent background within the spectral region of the azide probe for H_2O/D_2O solutions. While this predictive model was developed for water/D_2O solutions, it can be potentially applied to other protic solvent. For example, the azide probe in methanol was determined to have a population relaxation of 2.4 ± 0.2 ps via a magic-angle pump-probe measurement (data not shown). Using the average optical density of methanol in a 25 μm spacer, 0.055, the semi-empirical prediction of the lifetime was calculated to be 1.7 ± 0.2 ps, which is in reasonable agreement with the experiment.

The population relaxation times measured by magic-angle pump-probe spectroscopy were compared to those obtained via phase-resolved heterodyne-detected transient grating and the intensity decays of 2D IR spectroscopies. Provided the detection window is sufficiently long, the transient grating technique can be used to determine the reorientation time (T_R) in addition to the population relaxation time (T_1)[39]. Decay profiles of the azide probe in H_2O and D_2O obtained using transient grating spectroscopy are seen in the left panel of Figure 4. In water, T_1 is 0.58 ±

0.05 ps and T_R is 0.9 ± 0.2 ps, in good agreement to past studies[35,39]. For D_2O, the trace of the spectra was fitted to a single exponential, yielding a decay constant of 2.4 ± 0.5 ps, which closely matches the magic-angle pump probe. Past studies by Hochstrasser and coworkers have reported 7.1 ps [35] for the reorientation relaxation of azide in D_2O. Thus, the 6 ps collection window used here is likely not long enough to fully capture this longer reorientation component. Finally, the right panel of Figure 4 shows the 2D IR intensity decays of azide in water and D_2O, which were found to be 0.50 ± 0.01 ps and 2.06 ± 0.06 ps, respectively. These values closely resemble those obtained from the pump-probe (4% and 7% difference for water and D_2O, respectively) and transient grating (15% difference for both water and D_2O) measurements, suggesting that the 2D IR intensity decay of the $\nu = 0 \rightarrow \nu = 1$ transition can be used as good approximation for the vibrational relaxation times.

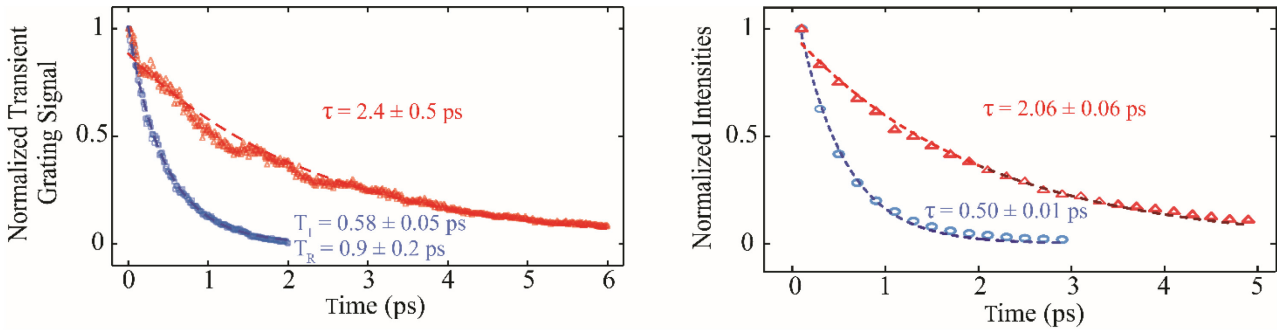

Figure 4. (Left) Kinetic traces and fits of transient grating spectra of NaN_3 in (blue circles) water and (red triangles) D_2O. (Right) Kinetic traces and fits of 2D IR intensity decay of NaN_3 in (blue circles) water and (red triangles) D_2O.

4. Conclusions

This study has demonstrated the importance of considering the spectral density of the solvent when estimating its influence on the vibrational dynamics of a solute probe. Armed with this knowledge, the proper solution of D_2O and water can be chosen to provide a sufficient window of observation for 2D IR measurements. Our results demonstrate that the frequency-frequency correlation decay does not change considerably under various D_2O/water ratios, i.e. with increasing spectral density. However, the vibrational lifetime of the azide transition is significantly influenced by the composition of the D_2O/water solution. Specifically, we observed a ~4.5-fold increase in vibrational lifetime in deuterated water compared to water, and we established a linear correlation between the vibrational lifetime and the average solvent spectral density around the azide transition. These results not only provide valuable insight into the importance of considering the role of the solvent in energy dissipation pathways for a vibrational probe of interest, but also propose a semi-empirical model to predict vibrational lifetimes based on the solvent spectral density. Although our study focused on a small-molecule system, the observed bath coupling model can provide a guide for tuning vibrational lifetimes in larger biomolecular systems. Overall, this work highlights the significance of understanding the spectral density of the solvent in studying energy dissipation pathways and vibrational dynamics in complex molecular systems.

AUTHOR INFORMATION

Notes

The authors declare no competing financial interests.

ACKNOWLEDGMENT

M.J.T., D.C.M. and M.H. acknowledge the NSF for the financial support of this work through CHE-2102275.

References

[1] Z. Getahun, C.Y. Huang, T. Wang, B. De Leon, W.F. DeGrado, F. Gai, J Am Chem Soc 125 (2003) 405.

[2] M. Hassani, C.J. Mallon, J.N. Monzy, A.J. Schmitz, S.H. Brewer, E.E. Fenlon, M.J. Tucker, J Chem Phys 158 (2023).

[3] F. Chalyavi, P.H. Gilmartin, A.J. Schmitz, M.W. Fennie, M.J. Tucker, Angew Chem Int Ed Engl 57 (2018) 7528.

[4] A.J. Schmitz, D.G. Hogle, X.S. Gai, E.E. Fenlon, S.H. Brewer, M.J. Tucker, J Phys Chem B 120 (2016) 9387.

[5] X.S. Gai, B.A. Coutifaris, S.H. Brewer, E.E. Fenlon, Phys Chem Chem Phys 13 (2011) 5926.

[6] B.A. Lindquist, K.E. Furse, S.A. Corcelli, Phys Chem Chem Phys 11 (2009) 8119.

[7] M.M. Waegele, R.M. Culik, F. Gai, J Phys Chem Lett 2 (2011) 2598.

[8] C. Fang, J.D. Bauman, K. Das, A. Remorino, E. Arnold, R.M. Hochstrasser, Proc Natl Acad Sci U S A 105 (2008) 1472.

[9] J.K. Chung, M.C. Thielges, M.D. Fayer, Proc Natl Acad Sci U S A 108 (2011) 3578.

[10] S. Bagchi, S.G. Boxer, M.D. Fayer, J Phys Chem B 116 (2012) 4034.

[11] K.I. Oh, J.H. Lee, C. Joo, H. Han, M. Cho, J Phys Chem B 112 (2008) 10352.

[12] I.T. Suydam, C.D. Snow, V.S. Pande, S.G. Boxer, Science 313 (2006) 200.

[13] R. Bloem, K. Koziol, S.A. Waldauer, B. Buchli, R. Walser, B. Samatanga, I. Jelesarov, P. Hamm, J Phys Chem B 116 (2012) 13705.

[14] B. Lee, B.M. Papoutsis, N.Y. Wong, J. Piacentini, C. Kearney, N.A. Huggins, N. Cruz, T.T. Ng, K.H. Hao, J.S. Kramer, E.E. Fenlon, P.S. Nerenberg, C.M. Phillips-Piro, S.H. Brewer, J Phys Chem B 126 (2022) 8957.

[15] M.J. Tucker, Z. Getahun, V. Nanda, W.F. DeGrado, F. Gai, J Am Chem Soc 126 (2004) 5078.

[16] A. Ghosh, M.J. Tucker, F. Gai, J Phys Chem B 118 (2014) 7799.

[17] F. Chalyavi, O. Adeyiga, J.M. Weiner, J.N. Monzy, A.J. Schmitz, J.K. Nguyen, E.E. Fenlon, S.H. Brewer, S.O. Odoh, M.J. Tucker, J Chem Phys 152 (2020) 074201.

[18] M.M. Waegele, M.J. Tucker, F. Gai, Chem Phys Lett 478 (2009) 249.

[19] M.J. Tucker, X.S. Gai, E.E. Fenlon, S.H. Brewer, R.M. Hochstrasser, Phys Chem Chem Phys 13 (2011) 2237.

[20] K.-I. Oh, J.-H. Lee, C. Joo, H. Han, M. Cho, The Journal of Physical Chemistry B 112 (2008) 10352.

[21] J.N. Bandaria, S. Dutta, S.E. Hill, A. Kohen, C.M. Cheatum, J Am Chem Soc 130 (2008) 22.

[22] J.Y. Park, H.J. Kwon, S. Mondal, H. Han, K. Kwak, M. Cho, Phys Chem Chem Phys 22 (2020) 19223.

[23] H. Taskent-Sezgin, J. Chung, P.S. Banerjee, S. Nagarajan, R.B. Dyer, I. Carrico, D.P. Raleigh, Angew Chem Int Ed Engl 49 (2010) 7473.

[24] C.G. Bazewicz, M.T. Liskov, K.J. Hines, S.H. Brewer, J Phys Chem B 117 (2013) 8987.

[25] P. Pagano, Q. Guo, A. Kohen, C.M. Cheatum, J Phys Chem Lett 7 (2016) 2507.

[26] A. Ghosh, M.J. Tucker, R.M. Hochstrasser, J Phys Chem A 115 (2011) 9731.

[27] A.L. Le Sueur, R.E. Horness, M.C. Thielges, Analyst 140 (2015) 4336.

[28] J.J. Loparo, S.T. Roberts, A. Tokmakoff, J Chem Phys 125 (2006) 194521.

[29] A. Ghosh, J.S. Ostrander, M.T. Zanni, Chem Rev 117 (2017) 10726.

[30] A.J. Schmitz, H.D. Pandey, F. Chalyavi, T. Shi, E.E. Fenlon, S.H. Brewer, D.M. Leitner, M.J. Tucker, J Phys Chem A 123 (2019) 10571.

[31] S. Bagchi, A.K. Charnley, A.B. Smith III, R.M. Hochstrasser, J Phys Chem B 113 (2009) 8412.

[32] I.V. Rubtsov, R.M. Hochstrasser, Journal of Physical Chemistry B 106 (2002) 9165.

[33] J.C. Owrutsky, D. Raftery, R.M. Hochstrasser, Annu Rev Phys Chem 45 (1994) 519.

[34] A.M. Woys, S.S. Mukherjee, D.R. Skoff, S.D. Moran, M.T. Zanni, J Phys Chem B 117 (2013) 5009.

[35] M. Li, J. Owrutsky, M. Sarisky, J.P. Culver, A. Yodh, R.M. Hochstrasser, The Journal of Chemical Physics 98 (1993) 5499.

[36] F. Chalyavi, D.G. Hogle, M.J. Tucker, J Phys Chem B 121 (2017) 6380.

[37] C.-Y. Huang, Z. Getahun, Y. Zhu, J.W. Klemke, W.F. DeGrado, F. Gai, Proceedings of the National Academy of Sciences 99 (2002) 2788.

[38] Y.S. Kim, J. Wang, R.M. Hochstrasser, The Journal of Physical Chemistry B 109 (2005) 7511.

[39] G.Y. Jin, Y.S. Kim, The Journal of Physical Chemistry A 121 (2017) 1007.

[40] L. De Marco, W. Carpenter, H. Liu, R. Biswas, J.M. Bowman, A. Tokmakoff, The Journal of Physical Chemistry Letters 7 (2016) 1769.

[41] P.K. Verma, A. Kundu, M.S. Puretz, C. Dhoonmoon, O.S. Chegwidden, C.H. Londergan, M. Cho, The Journal of Physical Chemistry B 122 (2018) 2587.

[42] S. Park, D.E. Moilanen, M.D. Fayer, The Journal of Physical Chemistry B 112 (2008) 5279.

[43] T. Yagasaki, S. Saito, Accounts of Chemical Research 42 (2009) 1250.

[44] J.J. Loparo, S.T. Roberts, A. Tokmakoff, The Journal of Chemical Physics 125 (2006) 194522.

[45] S.H. Schneider, H.T. Kratochvil, M.T. Zanni, S.G. Boxer, The Journal of Physical Chemistry B 121 (2017) 2331.

[46] D.G. Kuroda, R.M. Hochstrasser, Physical Chemistry Chemical Physics 14 (2012) 6219.

[47] M.T. Zanni, M.C. Asplund, R.M. Hochstrasser, The Journal of Chemical Physics 114 (2001) 4579.

[48] E.E. Fenn, D.B. Wong, C.H. Giammanco, M.D. Fayer, The Journal of Physical Chemistry B 115 (2011) 11658.

[49] K. Kwak, S. Park, I.J. Finkelstein, M.D. Fayer, The Journal of Chemical Physics 127 (2007) 124503.

[50] Y.S. Kim, R.M. Hochstrasser, The Journal of Physical Chemistry B 113 (2009) 8231.